CHEMISTRY OF MATERIALS
Article
Cite This: Chem. Mater. 2017, 29, 9819-9828
pubs.acs.org/cm

Cubine, a Quasi Two-Dimensional Copper−Bismuth Nanosheet

Maximilian Amsler,*,† Zhenpeng Yao, and Chris Wolverton*

Department of Materials Science and Engineering, Northwestern University, Evanston, Illinois 60208, United States

ABSTRACT: We report on the discovery of a quasi two-dimensional copper−bismuth nano sheet from *ab initio* calculations, which we call cubine. According to our predictions, single layers of cubine can be isolated from the recently reported high-pressure CuBi bulk material at an energetic cost of merely ≈20 meV/Å^2, comparable to values to separate single layers of graphene from graphite. Our calculations suggest that cubine has remarkable electronic and electrochemical properties: It is a superconductor with a moderate electron−phonon coupling $\lambda = 0.5$, leading to $T_c \approx 1$ K, and can be readily intercalated with lithium with a high diffusibility, rendering it a promising candidate material to boost the rate capacity of current electrodes in lithium-ion batteries.

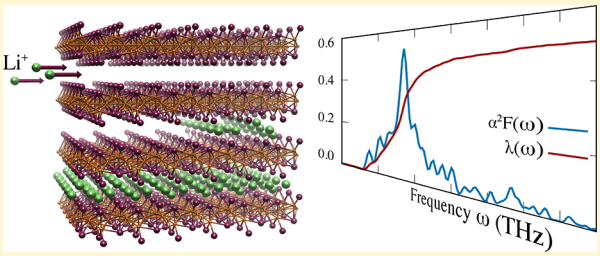

INTRODUCTION

Since the first successful exfoliating of graphene in 2004,[1−4] intense research has been devoted to the synthesis and characterization of two-dimensional (2D) materials. Meanwhile, various 2D materials have been discovered, ranging from graphene analogues such as silicene[5−8] to phosphorene[9] and borophene,[10−13] transition metal oxides,[14,15] transition metal dichalcogenides,[16,17] and transition metal carbinides/nitrides.[18,19] Due to their diverse properties, 2D materials have been considered for many industrially relevant applications, including nanoelectronics, optoelectronics, and photonics,[20−24] but also in the field of energy storage. For metal-ion batteries, materials that can host Li^+ or Na^+ at high densities are of particular interest, a market currently dominated by carbonaceous (*e.g.*, graphite and hard carbon) and layered materials (*e.g.*, $LiCoO_2$).[25] Two-dimensional materials are promising alternatives since they exhibit compelling ion transport and storage characteristics due to their open 2D channels and high specific surface areas with a large number of active sites.[25] Furthermore, since 2D materials only exhibit weak interlayer bonding *via* van der Waals (vdW) forces, unfavorable, large changes in their volumes during the intercalation and deintercalation of lithium ions are alleviated. Two-dimensional materials can also serve as functional substrates for incorporating active materials to improve the electrical and ionic conductivity of electrodes[3,26] and are promising candidates for applications in nanostructured supercapacitors.[27]

Theoretical efforts to identify potential new 2D materials have been aimed at screening large databases of crystalline materials for low-dimensional structural patterns.[28−30] Commonly, simple geometrical criteria such as large interlayer spacings are used to identify 2D units that could be separated through mechanical exfoliation. The recently discovered Cu−Bi intermetallics[31−35] have attracted considerable attention due to such low-dimensional structural features, including 1D channels and 2D voids.[31−33] Despite the strong immiscibility at ambient pressure,[34] Cu−Bi binary compounds have been known to form at high pressures since the early 1960s, exhibiting superconducting properties with a T_c between 1.33 and 1.40 K.[36] In 2016, a $Cu_{11}Bi_7$ compound was reported to form at moderate pressures, which crystallizes in a hexagonal structure with a T_c of 1.36 K.[31] Recently, another high-pressure phase in the Cu−Bi system at the equiatomic composition, CuBi, was discovered with an orthorhombic unit cell.[32,33] Despite the dissimilarities in their crystal structures, both $Cu_{11}Bi_7$ and CuBi share a common structural motif, namely, the formation of voids to host the lone electron pairs (LEP) of the two nonbonding Bi 6s electrons that form in the vicinity of the bismuth atoms. In contrast to $Cu_{11}Bi_7$, which exhibits channels laced by LEP, CuBi forms a layered structure of alternating Cu, Bi, and LEP sheets. The formation of this low-density phase is the more surprising since such materials strongly violate the common perception that high-pressure phases have high densities with short, strong interatomic bonds.

Here we investigate the CuBi compound using *ab initio* methods to unravel the unique structural features of CuBi and reveal its two-dimensional character. Based on our calculations, layers of CuBi are held together by weak vdW forces, and we demonstrate that single nanosheets of CuBi can be separated from the bulk material at an extremely low cost in energy, one that is comparable to values required to exfoliate graphene from graphite. The dynamical stability of CuBi nanosheets show that they are viable as metastable phases and could be potentially used as a new class of building blocks in 2D heterostructures with compelling physical properties: they are superconducting with a $T_c \approx 1$ K, could be used to intercalate Li atoms at low voltages, and hence make an interesting new electrode for Li-ion batteries.

Received: September 21, 2017
Revised: October 24, 2017
Published: October 24, 2017

DOI: 10.1021/acs.chemmater.7b03997
Chem. Mater. 2017, 29, 9819−9828

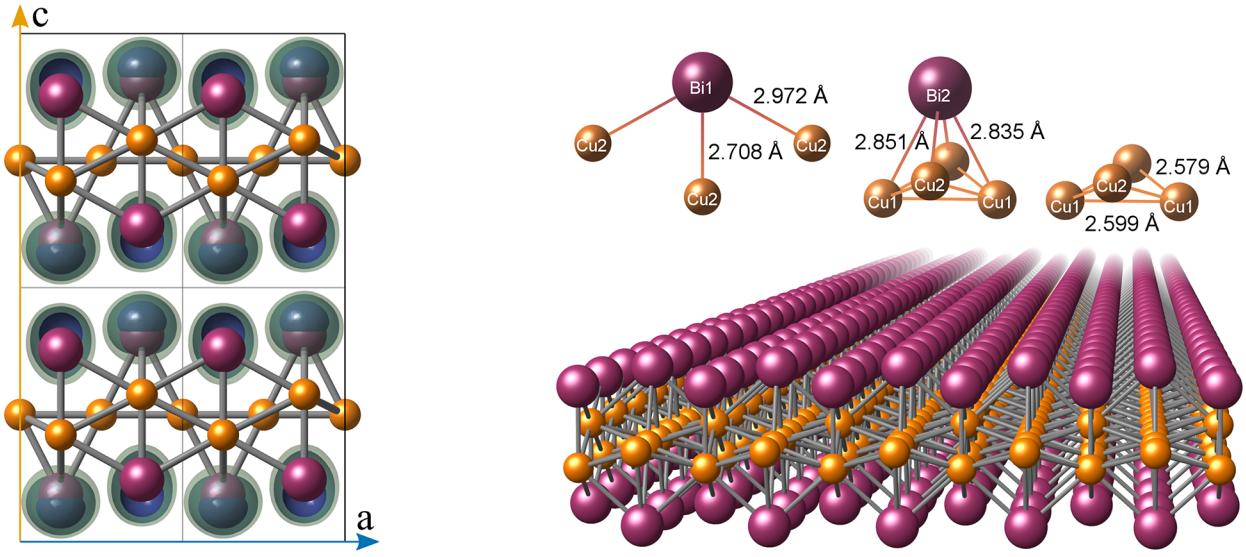

(a) Bulk CuBi (b) Bonding in cubine

Figure 1. (a) Bulk CuBi structure along the *b*-axis together with the isosurfaces of the ELF drawn at values of 0.9, 0.8, and 0.7 in purple, blue, and green, respectively. (b) Single sheet of cubine, exfoliated from CuBi, along the *a*-axis, together with the interatomic bonds. The two symmetrically inequivalent atoms Bi1 and Bi2 are attached to the buckled triangular sheet of Cu through three and four bonds, respectively. The core Cu sheet itself consists of a triangular lattice with two distinct short Cu−Cu bonds. In all figures, Cu and Bi atoms are denoted by orange (small) and purple (large) spheres.

RESULTS AND DISCUSSION

The thermodynamic stability of a solid state compound is governed by the Gibbs free energy, $G = E + pV - TS$, where the phase (or a combination of phases) with the lowest value is the stable state at a given pressure p and temperature T. At high pressure, the pV term becomes increasingly dominant, and therefore high-density polymorphs will be favored and a strong penalty is expected for layered, vdW bonded materials. The most prominent example for this behavior is carbon, where graphite, essentially consisting of layered graphene sheets and stable at ambient conditions, transforms into the dense cubic diamond structure at high pressures.[37] Similarly, N_2, a quasi 0D material at ambient pressure, turns into a polymeric phase at above 120 GPa,[38] following the trend that the dimensionality and density of accessible polymorphs increases with pressure.

The recently discovered high-pressure CuBi material, however, poses a puzzling exception to this general rule, since pieces of evidence indicate that CuBi is in fact a layered material with a strong 2D character. Experimentally, CuBi crystallizes in an orthorhombic cell with *Pmma* symmetry above 3.2 GPa, and its structure is shown in panel a of Figure 1 along the (010) direction. The atomic coordinates computed with the PBE functional are summarized in Table 1. According to our calculations, the lattice constants at 0 GPa are a = 5.204 Å, b = 4.263 Å, and c = 8.131 Å (see Table 2). While the values for a and b are in excellent agreement with experiments with errors of less than 0.5%, the c-vector is overestimated by roughly 3.3%.

Table 1. Atomic Coordinates of Bulk CuBi Computed with the PBE Functional

atom	Wyckoff position	x/a	y/b	z/c
Cu1	2d	0.000	0.500	0.500
Cu2	2e	0.250	0.000	0.579
Bi1	2e	0.250	0.000	0.245
Bi2	2f	0.250	0.500	0.815

A very similar behavior is observed in graphite,[39] where the interlayer distance is also severely overestimated, a first indication of the 2D character of CuBi. Furthermore, in both systems, this overestimation can be corrected by employing the LDA functional (due to its tendency of overbinding) or by using dispersion corrected PBE functionals as shown in Table 2. These findings clearly indicate that the interlayer interactions in CuBi are vdW mediated, a characteristic feature of layered 2D materials.

We can also see that CuBi is a layered material from a simple geometric argument. The main structural motif consists of layers of a buckled triangular sheet composed purely of Cu atoms in the a−b plane, with two unique Cu−Cu bonds. Along the b-direction the bond length is 2.601 Å, whereas along the a-direction it is 2.580 Å. Bi atoms are attached to both sides of these Cu sheets along the c-direction. Two further symmetrically inequivalent bonds are formed between Bi1 and Cu at distances of 2.716 and 2.969 Å, respectively, while Bi2 forms bonds with Cu at distances of 2.868 and 2.873 Å, respectively. No apparent bonds are formed between the Bi atoms, and all Bi−Bi distances are significantly larger than the sum of the covalent radii. In particular, the distance between the layers of Bi is 3.98 Å, clearly indicating that the bonding between the layers is neither covalent nor ionic. Furthermore, the electron localization function in Figure 1 shows no Bi−Bi bonds but instead reveals that stereochemically active LEP are interlaced between the Bi layers.

A detailed analysis of the lattice vibrations provides further evidence for the 2D character of CuBi. Figure 2a shows the phonon dispersion together with the path in the first Brillouin zone. We identify three specific features in the phonon band structure that are characteristic for quasi 2D materials. First, the lowest energy acoustic branch (yellow) shows a quadratic behavior as $q \rightarrow \Gamma$ along the in-plane directions X−Γ and Y−Γ, typical for 2D materials that exhibit a single flexural phonon branch with quadratic dispersion.[40] Second, the very flat bands

DOI: 10.1021/acs.chemmater.7b03997
Chem. Mater. 2017, 29, 9819−9828

Table 2. Lattice Parameters (Å) for CuBi and Graphite in Their Crystalline Phase (Columns 3−5) and as Isolated Layers of Cubine and Graphene (Columns 6 and 7) Using Various Exchange−Correlation Functionals[a]

		bulk			sheet		
	method	*a*	*b*	*c*	*a*	*b*	E_i
cubine	PBE	5.204	4.263	8.131	5.197	4.272	4
	LDA	5.085	4.125	7.817	5.055	4.145	21
	D2	5.161	4.235	7.916	5.164	4.221	31
	D3	5.066	4.250	7.901	5.054	4.255	20
	D3-BJ	5.151	4.181	7.743	5.095	4.209	24
	TS-HP	5.061	4.243	7.907	5.056	4.245	20
	dDsC	5.164	4.210	7.895	5.130	4.227	14
	exp[32]	5.207	4.242	7.876	–	–	–
	exp[33]	5.189	4.231	7.866	–	–	–
graphene	PBE[39]	2.466		8.755	–		1
	PBE[48]	–		–	2.465		–
	LDA[49]	2.460		6.660	–		9
	LDA[50]	–		–	2.460		–
	D2[39]	2.461		6.444	–		21
	D3[39]	2.464		6.965	–		18
	exp[51]	2.46		–	–		20 ± 2
	exp[52]	2.46		6.70	–		13

[a]The last column contains the interlayer energies E_i (meV/Å^2). The following abbreviations were used for the various dispersion corrected PBE functionals: Grimme D2 (D2),[43] Grimme D3 without (D3)[44] and with (D3-BJ)[45] Becke−Johnson dampening, Tkatchenko−Scheffler method with iterative Hirshfeld partitioning (TS-HP),[46] and Steinmann's density-dependent dispersion energy correction dDsC.[47].

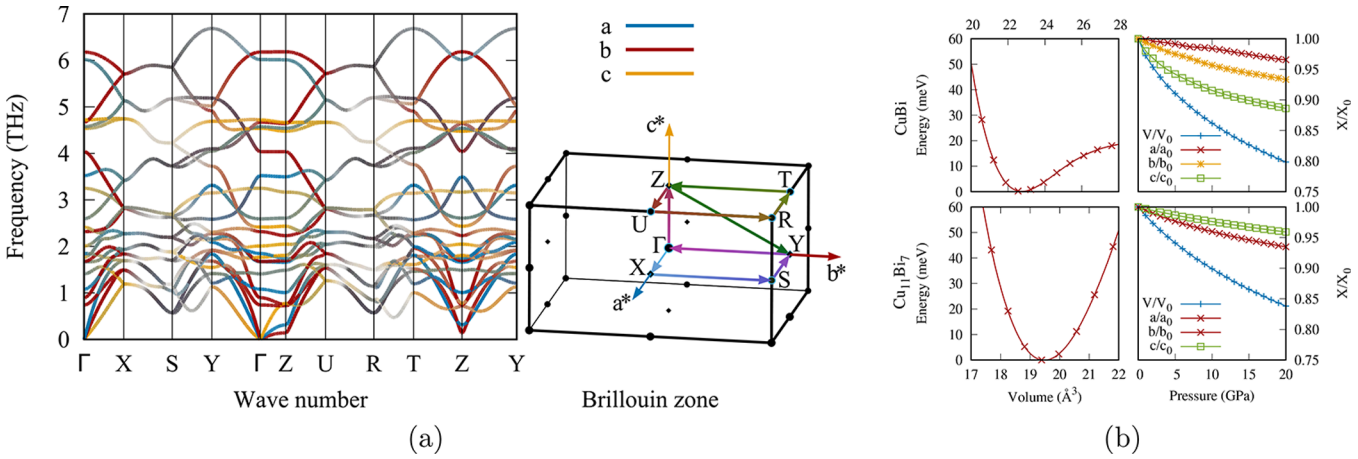

Figure 2. (a) Phonon dispersion of bulk CuBi along a path in the first Brillouin zone, computed with the PBE functional. The colors indicate the contribution of the vibrational eigenmodes along the three crystal lattices a, b, and c. (b, left) Energy per atom as a function of volume, top for CuBi and bottom for $Cu_{11}Bi_7$; (right) evolution of the lattice parameters and the unit cell volume normalized to the ambient pressure values, for CuBi and $Cu_{11}Bi_7$ at the top and bottom, respectively.

along Γ−*Z* with essentially zero dispersion can be directly attributed to extremely weak interactions between the layers. Third, the two lowest energy branches along Γ−*Z* are dominated by collective in-plane vibrations of the atoms in the *a*- and *b*-directions. This behavior is shown by the color coding based on the magnitude of the projected vibrational eigendisplacements along the three lattice vector components.

The anisotropic compressibility and strong anharmonicity of CuBi is the fourth evidence for its 2D character. Figure 2b compares the structural parameters upon compression and expansion of CuBi with the recently discovered $Cu_{11}Bi_7$ phase.[31] While the latter exhibits a roughly quadratic dependence of the energy on the volume, CuBi behaves strongly anharmonically, similar to graphite.[41] The right panels in Figure 2b show the pressure dependence of the normalized unit cell volumes and the cell parameters upon compression of CuBi and $Cu_{11}Bi_7$. In contrast to $Cu_{11}Bi_7$, the change in the lattice vectors of CuBi is highly anisotropic, with a higher compressibility along the *c*-direction compared to *a* and *b*. This high compressibility is partially responsible for the fact that CuBi becomes thermodynamically stable at increased pressures: although bulk CuBi has a positive heat of formation of ΔE = 48 meV/atom (PBE) at 0 K and ambient pressure, the Gibbs free formation energy ΔG becomes negative at elevated pressures and temperatures when taking into account vibrational entropy, as discussed in detail in ref 33.

Based on all these properties supporting the 2D character of CuBi, we investigated if a single layer of CuBi, so-called cubine, is in fact viable. The two necessary criteria that need to be satisfied are that cubine is dynamically stable and that there is only a moderate-to-weak energy penalty for isolating single sheets. A vacuum layer of 12 Å between the sheets was

DOI: 10.1021/acs.chemmater.7b03997
Chem. Mater. 2017, 29, 9819−9828

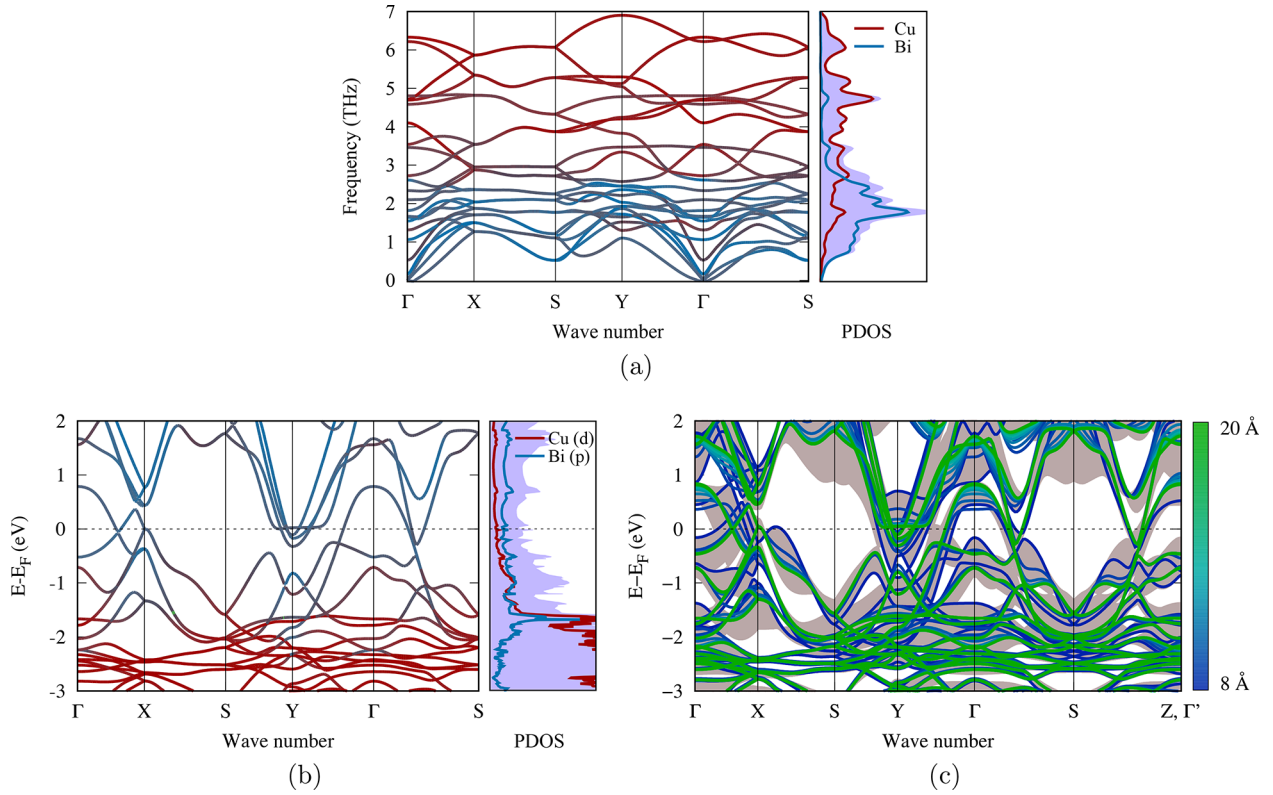

Figure 3. (a) Phonon band structure of the quasi 2D isolated cubine sheet together with the partial density of states (PDOS) using the PBE functional, indicating that no imaginary modes arise within the complete 2D Brillouin zone. The red and blue color coding denotes the modes dominated by Cu and Bi vibrations, respectively. The shaded area in the PDOS represents the total density of states. (b) Electronic band structure of cubine using PBE, where the colors indicate the band character projected onto the Cu and Bi atoms in red and blue, respectively. The shaded area in the right panel represents the total density of states, whereas the red and blue lines denote the Cu 3d and Bi 6p contributions, respectively. (c) Evolution of the band structure as a function interlayer separation, color-coded from 8 (blue) to 20 Å (green) along a path in the bulk CuBi Brillouin zone. The shaded gray area corresponds to the projected bands of the bulk structure onto the 2D Brillouin zone. Note that Z and Γ coincide in the limit of infinitely large c-vectors, as shown by the segment $S-(Z, \Gamma')$.

introduced to separate the single sheets of cubine, followed by a relaxation of the atomic coordinates and the in-plane lattice vectors. The bond lengths in cubine only slightly change upon relaxation as shown in Figure 1b, with Cu−Cu distances of 2.599 Å along the a- and 2.579 Å along the b-direction, respectively. The Cu−Bi1 bonds change from 2.716 to 2.708 Å, and from 2.969 to 2.972 Å, respectively, while the Cu−Bi2 bonds decrease from 2.868 to 2.851 Å and from 2.873 to 2.835 Å, respectively. Figure 3a shows the phonon dispersion in the 2D Brillouin zone of this relaxed structure. No imaginary phonons are present, indicating that single sheets of cubine are dynamically stable. The color coding of the bands and the partial density of states show that two frequency regions can be clearly distinguished. The low-frequency regime below ≈3 THz is strongly dominated by vibrations of the heavy Bi atoms, whereas the lighter Cu atoms contribute to the high-energy phonons.

To assess if cubine can be isolated, we computed the interlayer binding energy E_i between the individual sheets according to $E_i = \frac{E_{\text{sheet}} - E_{\text{bulk}}}{A}$, where E_{bulk} is the total bulk energy and A is the area spanned by the in-plane lattice vectors. E_{slab} is the energy of a single layer of cubine, evaluated by introducing a vacuum layer of 12 Å between the individual sheets. The PBE functional results in an extremely low value in E_i of merely 4 meV/Å^2. Using this value, a single cubine sheet has a positive formation energy of 68 meV/atom with respect to the elements. Since semilocal DFT does not account for vdW interactions, the real interlayer energy might be significantly higher. Indeed, our values of E_i by using functionals that (empirically) take into account dispersion energies, are overall higher than PBE and lie consistently in the range of ≈15−30 meV/Å^2 (see Table 2). These values are close to the interlayer energies of graphite and other (quasi) 2D materials,[28,29,42] and therefore strongly support the potential of exfoliating cubine from bulk in analogy to graphene.[1]

Table 2 also provides two conclusive pieces of evidence that CuBi is indeed a layered material where cubine sheets interact with each other through vdW forces. First, all vdW functionals consistently predict lower c-vectors compared to PBE by 3−5%, which also agree significantly better with the experimental values. Second, evidence is directly given by the interlayer binding energies: since PBE does not describe any vdW interactions, the difference in the binding energy between a vdW functional and PBE, $\Delta_{E_i} = E_i^{\text{vdW}} - E_i^{\text{PBE}}$, can be directly attributed to the dispersion forces. The positive values in Δ_{E_i} for all vdW functionals show that in bulk CuBi the layers of cubine are held together by vdW forces.

In order to compare with available literature data, we screened the large 2D materials database at www.materialsweb.org for structures similar to cubine, but none of the 15 binary AB prototype structures[29] matches its space group symmetry. However, two compounds have similar structural motifs of a

DOI: 10.1021/acs.chemmater.7b03997
Chem. Mater. 2017, 29, 9819−9828

core Cu sheet between layers of a second atomic species, namely, CuTe and CuBr. In contrast to cubine, CuBr has a completely planar Cu layer (space group *P*4/*nmm*), while CuTe exhibits a slightly different stacking geometry (space group *Pmmn*). Hence, the structure of cubine (space group *Pmma*) is presumably novel, and we propose it to be added to the database as the 16th member of *AB* prototypes.

Similar to its bulk counterpart, cubine is metallic as illustrated by the band structure in Figure 3b with a rather low density of states (DOS) at the Fermi level. As expected, the strongest contributions at the Fermi level stem from the Cu 3d and Bi 6p states. The 2 Bi 6s electrons of the stereochemically active LEP are buried deep below the valence bands. Compared to the DOS of the bulk CuBi reported in ref 32, cubine in vacuum has a slightly lower contribution of Bi states at the Fermi level. We attribute this discrepancy in the DOS to the electronic interaction between the Bi atoms facing each other when the cubine sheets are stacked on top of each other in bulk CuBi. The gradual change of the electronic band structure due to quantum confinement as the bulk CuBi transform into isolated sheets of cubine is shown in Figure 3c. At every value of the *c*-vector, the in-plane cell vectors and all atomic coordinates were fully relaxed. The bands along $\Gamma-S$ and $S-Z$ become symmetric in the limit of large *c*-vectors (green), corresponding to the 2D sheet of cubine, while the bands of the bulk phase show an asymmetric dispersion (blue). The shaded area corresponds to the projected bands of the bulk structure onto the 2D Brillouin zone (where the bands were integrated along the out-of-plane direction in the reciprocal space) showing the effect of dispersion along the nonperiodic direction in the bulk phase.

This evolution of the electronic structure is also reflected in a change of the superconducting transition temperatures in the cubine nanosheet. Figure 4 shows the Eliashberg spectral

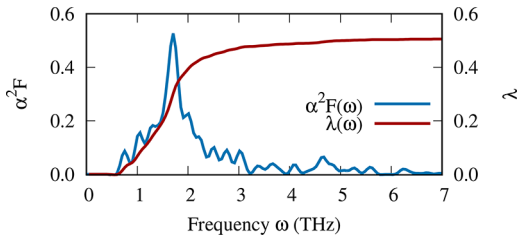

Figure 4. Eliashberg spectral function $\alpha^2F(\omega)$ of cubine together with the integrated electron–phonon coupling parameter $\lambda(\omega)$ as a function of the phonon frequency ω computed with the PBE functional.

function $\alpha^2F(\omega)$ together with the integrated electron–phonon coupling parameter $\lambda(\omega)$ using the PBE functional. $\alpha^2F(\omega)$ exhibits a strong peak around 2 THz, and $\lambda(\omega)$ increases sharply in the range of 0–2 THz. A comparison with the PDOS in Figure 3a reveals that these low energy phonon modes stem primarily from the vibration of the heavy Bi atoms. The resulting coupling strength of $\lambda = 0.50$ is rather weak, and considerably lower than for the bulk material, $\lambda = 0.67$.[33] Depending on the value of the empirical Coulomb pseudopotential μ^*, the predicted superconducting temperature ranges from 0.6 to 1.0 K. It is well-known that computed values of T_c are sensitive to the choice of the exchange–correlation functional. To estimate the error that arises from the somewhat arbitrary choice of the functional, we repeated the electron–phonon coupling calculation with the LDA functional. Slightly lower values of T_c were obtained with LDA, as indicated by the results summarized in Table 3.

Table 3. Electron–Phonon Coupling Parameters for Both the PBE and the LDA Exchange–Correlation Functionals and the Resulting Superconducting Transition Temperatures T_c for Different Values of μ^*

	T_c (K)					
	$\mu^* = 0.10$	$\mu^* = 0.11$	$\mu^* = 0.12$	$\mu^* = 0.13$	λ	ω_{log} (K)
PBE	1.0	0.8	0.7	0.6	0.50	80
LDA	0.7	0.6	0.5	0.4	0.45	86

Due to their large surface areas, 2D materials such as graphite have recently attracted interest as additives to enhance the performance of electrodes in metal-ion batteries.[53−55] Here, we investigate the potential of using cubine sheets in lithium-ion batteries by studying the adsorption of Li atoms directly on its surface. We identified three symmetrically distinct sites on cubine where Li can be deposited, shown in the top right inset of Figure 5a. We systematically explored all possible decorations of these three sites on both sides of a cubine sheet in one unit cell of Li_xCuBi. For $x = 0.25$ (*i.e.*, one Li per cell), the most favorable adsorption sites are A and B, which are located between four Bi atoms and lead to adsorption energies per Li atom of 1.90 and 1.88 eV, respectively. Site C is energetically unfavorable and can only be occupied once both the A and B sites are completely filled at higher values of *x*. A full occupation of all sites results in Li_2CuBi, and a potential gravimetric charge density of 192.92 mA h/g. Figure 5a shows the lowest energy adsorption geometries together with the change in adsorption energies as a function of surface coverage.

In practical energy storage applications, the kinetics of the adsorbed species on a surface is an important factor in the rate of charge/discharge. Hence, we computed the diffusion barriers of Li along the geometrically distinct paths on the cubine sheet (Figure 5b). The lowest barrier was found for the pathway A–B with a height of merely 0.13 eV, which is 40% lower than the barrier between the two most stable adsorption sites of Li on graphene.[56] Since the A–B sites form a network on the surface connected through these low energy barriers, we expect that the Li atoms can diffuse at a high rate on the surface. The energy profile for the paths A–C and B–C show that the C site is indeed a stationary saddle point (between A–A and B–B sites), which only transforms into a local minimum once the A and B sites are occupied.

The very low interlayer binding energy, the large spacing of 3.98 Å (graphite, 3.35 Å) between the sheets, and the low diffusion barriers of Li on cubine also render bulk CuBi potentially an attractive candidate as a metal intercalation electrode. There are two symmetrically distinct interstitial sites per cell (inset of panel i, Figure 6a) with each 2-fold degeneracy between the cubine layers that can host four guest atoms in total. By fully occupying these sites with Li, Na, Mg, and Al, gravimetric (and volumetric) capacities of 96.46 mA h/g (493.25 mA h/mL), 92.45 mA h/g (472.75 mA h/mL), 184.27 mA h/g (942.27 mA h/mL), and 274.51 mA h/g (1403.72 mA h/mL) could be potentially achieved, respectively. Although the gravimetric capacities of bulk CuBi are rather moderate, the volumetric capacities are close to values of commercially used anode materials such as graphite (550 mA h/mL). Besides a high capacity, there is an increasing demand for electrode

DOI: 10.1021/acs.chemmater.7b03997
Chem. Mater. 2017, 29, 9819–9828

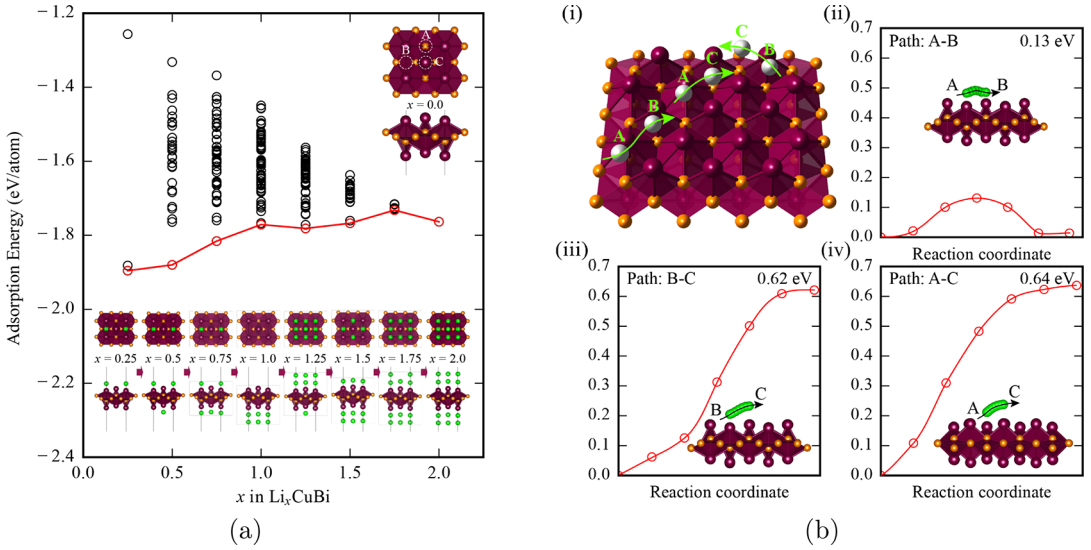

Figure 5. (a) Adsorption energies per Li atom of Li_xCuBi on a single sheet of cubine at various coverage densities x, where the red line connects the lowest energy configurations at a given x. The three distinct adsorption sites are denoted with A, B, and C (top right inset), and the lowest energy adsorption geometries at different surface coverages are shown by the insets at the bottom. (b) Calculated Li kinetics on a single sheet of cubine. Subpanel I shows the lithium-ion diffusion pathways on the surface. Subpanels ii–iv show the kinetic barriers calculated along geometrically distinct diffusion pathways: A–B, B–C, and A–C.

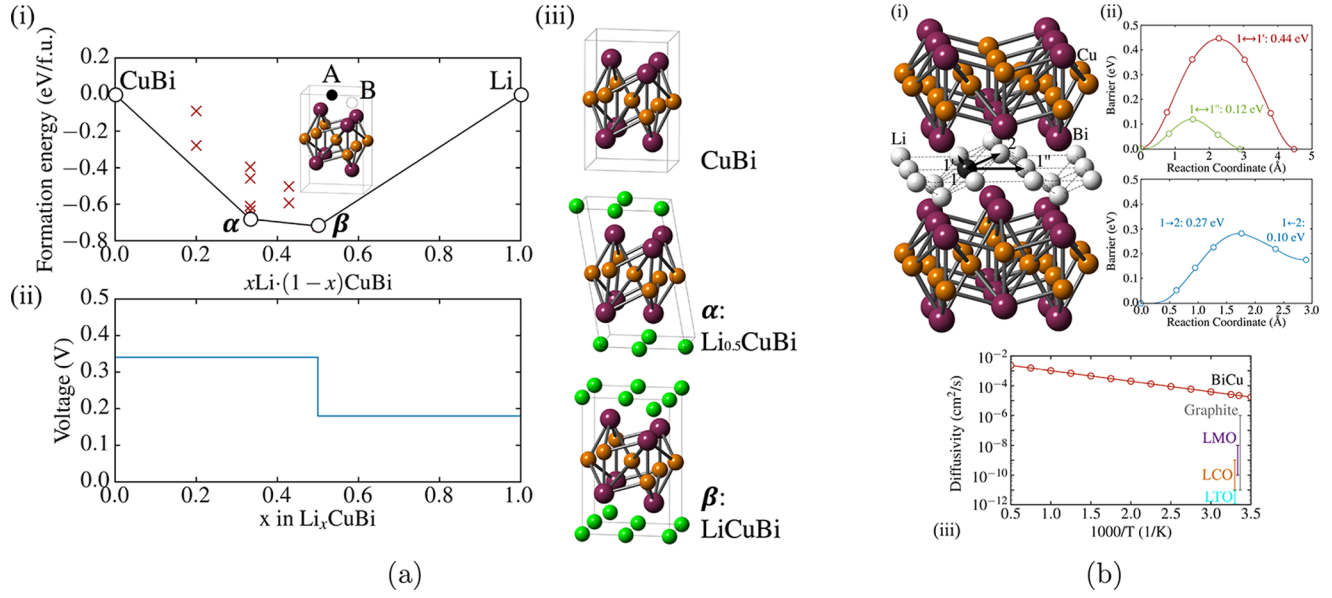

Figure 6. (a) PBE results of the CuBi-Li convex hull of stability as a function of lithium concentration (i) and the corresponding voltage profile (ii). Predicted structures of the intermediate phases are shown in iii. (b, i) Lithium-ion diffusion network through the interlayer space of CuBi; (ii) kinetic barriers calculated along geometrically distinct diffusion paths using PBE; (iii) calculated lithium-ion diffusivity as a function of temperature (attempt frequency, $\nu = 10^{13}$ s^{-1}), compared to state-of-the-art anodes (graphite and LTO ($Li_4Ti_5O_{12}$)) and cathodes (LCO ($LiCoO_2$) and LMO ($LiMn_2O_4$)), with experimental data adopted from refs 57 and 58.

materials with high rate capacities to improve battery power and to reduce the (re)charge time. To assess these charge/discharge and ion diffusion properties, we investigated the lithiation electrochemistry of CuBi. There are two intermediate phases on the CuBi–Li convex hull, where the end points are given by CuBi and elemental metallic Li, as shown in panel I of Figure 6a: $Li_{0.5}CuBi$ and LiCuBi. The corresponding voltage profile is shown in panel ii, with values in a fairly low range of 0.18–0.34 V, indicating that this material is more suitable as an anode material. During the whole lithiation process, the CuBi backbone remains completely intact with only a slight sliding of the cubine layers against each other around the concentration $Li_{0.5}CuBi$ (see panel iii in Figure 6a).

Furthermore, the interlayer diffusion of the Li atoms was investigated by computing the barriers along the geometrically distinct paths between the cubine layers (Figure 6b). The lowest among all barriers was found for the transition between the symmetrically equivalent 1 and 1″ sites with a value of merely 0.12 eV, which is even lower than the lowest barrier for the isolated cubine sheet. With all transition barriers at hand, a kinetic Monte Carlo simulation was carried out to estimate the lithium-ion diffusivity D. The values of D as a function of temperature are shown in Figure 6b(iii), calculated using a

DOI: 10.1021/acs.chemmater.7b03997
Chem. Mater. 2017, 29, 9819–9828

typical attempt frequency of $\nu = 10^{13}$ s^{-1}. We find a superior Li diffusivity of 3.8×10^{-5} cm^2/s at room temperature, more than 1 order of magnitude higher than state-of-the-art anodes (graphite, $D = 10^{-6}$–10^{-11} cm^2/s; $Li_4Ti_5O_{12}$ (LTO), $D = 10^{-11}$–10^{-12} cm^2/s) and cathodes ($LiCoO_2$ (LCO), $D = 10^{-8}$–10^{-10} cm^2/s; $LiMn_2O_4$ (LMO), $D = 10^{-9}$–10^{-11} cm^2/s).[57,58] This remarkable diffusivity renders CuBi a high-rate material that is capable of conducting Li faster than any known electrode material to date. Considering the high volumetric capacity together with the intriguing Li conductivity at relatively low cost, CuBi is a promising candidate to be used on its own in an anode for applications where space is limited and a high charge/discharge rate is required in electrical energy storage, *e.g.*, in electric vehicles and for peak load regulations of smart power grids. On the other hand, cubine with its large surface area and high number of active sites could be used as a component in composite anode and cathode materials (such as graphene) to improve their performance, *e.g.*, by increasing the rate capacity[59] and cyclability.[60]

In summary, we report on the discovery of a novel quasi 2D sheet, cubine. We present many pieces of compelling evidence to demonstrate that CuBi is indeed a layered material with weak vdW interactions between single cubine sheets. Since the interlayer energy is comparable to graphene, we predict that single sheets of cubine can be exfoliated from CuBi using similar techniques used to isolate graphene from graphite. As a single sheet, cubine is metallic with a moderate electron–phonon coupling, leading to superconducting transition temperatures in the range of around 0.6–1 K. Since it is dynamically stable, cubine can readily serve as a building block for heterostructured 2D materials, and its large surface area offers potential active sites for adsorbates such as Li atoms. The low energy barriers between the A and B sites allows a high diffusion of Li on cubine. Furthermore, we demonstrate that the bulk CuBi can be readily intercalated with lithium with a high ion diffusivity, rendering it a promising candidate for energy storage applications.

METHODS

Density functional theory (DFT) calculations were carried out within the projector augmented wave (PAW) formalism[61] as implemented in the VASP[62−64] package. Unless otherwise noted, we employed the Perdew–Burke–Ernzerhof (PBE) approximation[65] to the exchange–correlation potential. A plane-wave cutoff energy of 400 eV was used with a sufficiently dense *k*-point mesh to ensure a convergence of the total energy to within 1 meV/atom. Both the atomic and cell parameters were simultaneously relaxed until the maximal force components were less than 2 meV/Å and stresses less than 0.01 GPa. The structures were fully relaxed with the correct energy derivatives (Hellman–Feynman forces) of the respective exchange correlation functional.

The electron localization function (ELF), introduced by Becke *et al.*,[66] provides a convenient method to identify regions in space where electrons are strongly (or weakly) localized using DFT. The probability density $D(\mathbf{r})$ is defined in terms of the electron density $\rho(\mathbf{r})$ and the kinetic energy density $\tau(\mathbf{r}) = \frac{1}{2}\sum_i n_i|\nabla\psi_i(\mathbf{r})|^2$, where ψ_i are the single particle orbitals with the occupation numbers n_i, as $D(\mathbf{r}) = \tau(\mathbf{r}) - \frac{1}{8}\frac{|\nabla\rho(\mathbf{r})|^2}{\rho(\mathbf{r})}$. The dimensionless ELF is defined with respect to the probability density of the uniform electron gas $D_h(\mathbf{r})$ through $\mathrm{ELF} = \left(1 + \left[\frac{D(\mathbf{r})}{D_h(\mathbf{r})}\right]^2\right)^{-1}$, where ELF takes on values between 0 (not localized) to 1 (highly localized), and 0.5 for a localization identical to a uniform electron gas of the same density.

Phonon calculations were carried out with the frozen phonon approach as implemented in the PHONOPY package,[67] using sufficiently large supercells for converged thermal properties. To compute the vibrational contribution to the density of states, a dense mesh of 30 × 30 × 30 was used to sample the irreducible Brillouin zone.

The Quantum Espresso package[68] was used to compute the phonon-mediated superconducting properties. We used norm conserving FHI pseudopotentials and a plane-wave cutoff energy of 150 Ry. The Allan–Dynes modified McMillan's approximation of the Eliashberg equation[69] was used to estimate the superconducting temperature:

$$T_c = \frac{\omega_{\log}}{1.2}\exp\left[-\frac{1.04(1+\lambda)}{\lambda - \mu^*(1+0.62\lambda)}\right] \quad (1)$$

where μ^* is the Coulomb pseudopotential, λ is the overall electron–phonon coupling strength computed from the frequency-dependent Eliashberg spectral function $\alpha^2F(\omega)$, and $\omega_{\log}$ is the logarithmic average phonon frequency. A 4 × 4 × 1 *q*-mesh was used together with a denser 32 × 32 × 1 *k*-mesh for the 2D *Pmma* structure, resulting in a well-converged superconducting transition temperature T_c. A value of $\mu^* = 0.10$–0.13 was employed, which was shown to give values of T_c in excellent agreement with experimental results for the $Cu_{11}Bi_7$ superconductor.[31]

The Li adsorption process on the cubine single layer was computed using the non-equilibrium phase search method (NEPS)[70−72] by exploring geometrically distinct Li/vacancy configurations on all possible adsorption sites of the cubine surface at different compositions (Li/vacancy ratios). Starting with the cubine unit cell (Cu_4Bi_4) which has a total of eight empty sites where Li ions can adsorb, we generated all symmetrically distinct configurations using Enum[73,74] for a series of compositions $Li_x\square_{2-x}CuBi$ ($0 < x < 2$, $\square$ denoting vacancies). The total energies of all configurations were evaluated with the DFT settings described earlier. We also adopted the vdW-DF functional (optB88),[75] which employs a self-consistent van der Waals (vdW) correction. At each composition x the adsorption energy was computed according to

$$E_{\mathrm{ads}} = \frac{E(\mathrm{Li}_x\mathrm{CuBi}) - xE(\mathrm{Li}) - E(\mathrm{CuBi})}{x} \quad (2)$$

where the reference energy E(Li) of a single Li was evaluated in vacuum using a 10 Å × 10 Å × 10 Å supercell.

To simulate the lithiation process of bulk CuBi, the conventional cell was used to explore geometrically distinct potential Li sites between the cubine layers. All symmetrically inequivalent occupation of these sites was used as input structures and relaxed with respect to the atomic and cell variables using the PBE functional, resulting in energies as a function of Li/vacancy ratios, *i.e.*, the Li concentrations in Li_xCuBi. The formation energies were evaluated according to the following reaction: $CuBi + xLi \rightarrow Li_xCuBi$. The lithiation convex hull was constructed from the lowest formation energies at every composition, and only those intermediate phases which lie on the hull were considered, using metallic Li as a reference. The average lithiation/delithiation reaction voltage relative to Li/Li$^+$ is given by the negative of the reaction free energy per Li:[76]

$$\bar{V} = \frac{\Delta G_f}{F\Delta N_{\mathrm{Li}}} \quad (3)$$

where F is the Faraday constant, ΔN_{Li} is the amount of Li added/removed, and ΔG_f is the (molar) change in free energy of the reaction. The enthalpic (pV_m) contribution to G is of the order of 10 μeV per Li at atmospheric pressure and can be safely ignored, while the entropic contribution to the voltage was assumed to be small and was therefore neglected.[77] Hence, the total DFT $T = 0$ K internal energies (E) were used to approximate G:

$$\Delta G \approx \Delta E = E(\mathrm{Li}_x\mathrm{CuBi}) - E(\mathrm{CuBi}) - xE(\mathrm{Li}_{\mathrm{metal}}) \quad (4)$$

DOI: 10.1021/acs.chemmater.7b03997
Chem. Mater. 2017, 29, 9819–9828

where $E(Li_xCuBi)$, $E(CuBi)$, and $E(Li_{metal})$ are the total energies of Li_xBiCu, BiCu, and elemental Li, respectively. The lithium-ion diffusivity was studied using kinetic Monte Carlo (KMC) simulations using the Materials Interface package MINT[78,79] based on barriers computed through the climbing image nudged elastic band (*c*NEB) approach as implemented in the VASP TST package.[80−82]

AUTHOR INFORMATION

Corresponding Authors

*(M.A.) E-mail: amsler.max@gmail.com.
*(C.W.) E-mail: c-wolverton@northwestern.edu.

ORCID

Maximilian Amsler: 0000-0001-8350-2476
Chris Wolverton: 0000-0003-2248-474X

Present Address

†Laboratory of Atomic and Solid State Physics, Cornell University, Ithaca, NY 14853, USA.

Notes

The authors declare no competing financial interest.

ACKNOWLEDGMENTS

M.A. (band structure, interlayer energy, phonon, and superconductivity calculations) acknowledges support from the Novartis Universität Basel Excellence Scholarship for Life Sciences, the Swiss National Science Foundation (Grant Nos. P300P2-158407 and P300P2-174475). Z.Y. and C.W. (the Li intercalation, ion conductivity calculations, and overall leadership of this project) were supported as part of the Center for Electrochemical Energy Science (CEES), an Energy Frontier Research Center funded by the U.S. Department of Energy, Office of the Science, Basic Energy Science under Award No. DE-AC0206CH11. We gratefully acknowledge the computing resources from the Swiss National Supercomputing Center in Lugano (Project s700), the Extreme Science and Engineering Discovery Environment (XSEDE) (which is supported by National Science Foundation Grant No. OCI-1053575), the Bridges system at the Pittsburgh Supercomputing Center (PSC) (which is supported by NSF Award No. ACI-1445606), the Quest high-performance computing facility at Northwestern University, the National Energy Research Scientific Computing Center (DOE Grant No. DE-AC02-05CH11231), and Blues, a high-performance computing cluster operated by the Laboratory Computing Resource Center at Argonne National Laboratory.

REFERENCES

(1) Novoselov, K. S.; Geim, A. K.; Morozov, S. V.; Jiang, D.; Zhang, Y.; Dubonos, S. V.; Grigorieva, I. V.; Firsov, A. A. Electric Field Effect in Atomically Thin Carbon Films. *Science* **2004**, *306*, 666−669.

(2) Yoo, E.; Kim, J.; Hosono, E.; Zhou, H.-s.; Kudo, T.; Honma, I. Large Reversible Li Storage of Graphene Nanosheet Families for Use in Rechargeable Lithium Ion Batteries. *Nano Lett.* **2008**, *8*, 2277−2282.

(3) Wu, Z.-S.; Ren, W.; Wen, L.; Gao, L.; Zhao, J.; Chen, Z.; Zhou, G.; Li, F.; Cheng, H.-M. Graphene Anchored with Co3O4 Nanoparticles as Anode of Lithium Ion Batteries with Enhanced Reversible Capacity and Cyclic Performance. *ACS Nano* **2010**, *4*, 3187−3194.

(4) Wang, H.; Cui, L.-F.; Yang, Y.; Sanchez Casalongue, H.; Robinson, J. T.; Liang, Y.; Cui, Y.; Dai, H. Mn_3O_4−Graphene Hybrid as a High-Capacity Anode Material for Lithium Ion Batteries. *J. Am. Chem. Soc.* **2010**, *132*, 13978−13980.

(5) Takeda, K.; Shiraishi, K. Theoretical Possibility of Stage Corrugation in Si and Ge Analogs of Graphite. *Phys. Rev. B: Condens. Matter Mater. Phys.* **1994**, *50*, 14916−14922.

(6) Guzmán-Verri, G. G.; Lew Yan Voon, L. C. Electronic Structure of Silicon-Based Nanostructures. *Phys. Rev. B: Condens. Matter Mater. Phys.* **2007**, *76*, 075131.

(7) Cahangirov, S.; Topsakal, M.; Aktürk, E.; Şahin, H.; Ciraci, S. Two- and One-Dimensional Honeycomb Structures of Silicon and Germanium. *Phys. Rev. Lett.* **2009**, *102*, 236804.

(8) Vogt, P.; De Padova, P.; Quaresima, C.; Avila, J.; Frantzeskakis, E.; Asensio, M. C.; Resta, A.; Ealet, B.; Le Lay, G. Silicene: Compelling Experimental Evidence for Graphenelike Two-Dimensional Silicon. *Phys. Rev. Lett.* **2012**, *108*, 155501.

(9) Li, W.; Yang, Y.; Zhang, G.; Zhang, Y.-W. Ultrafast and Directional Diffusion of Lithium in Phosphorene for High-Performance Lithium-Ion Battery. *Nano Lett.* **2015**, *15*, 1691−1697.

(10) Amsler, M.; Botti, S.; Marques, M. A. L.; Goedecker, S. Conducting Boron Sheets Formed by the Reconstruction of the α-Boron (111) Surface. *Phys. Rev. Lett.* **2013**, *111*, 136101.

(11) Tang, H.; Ismail-Beigi, S. Novel Precursors for Boron Nanotubes: The Competition of Two-Center and Three-Center Bonding in Boron Sheets. *Phys. Rev. Lett.* **2007**, *99*, 115501.

(12) Tang, H.; Ismail-Beigi, S. First-Principles Study of Boron Sheets and Nanotubes. *Phys. Rev. B: Condens. Matter Mater. Phys.* **2010**, *82*, 115412.

(13) Lu, H.; Mu, Y.; Bai, H.; Chen, Q.; Li, S.-D. Binary Nature of Monolayer Boron Sheets from Ab Initio Global Searches. *J. Chem. Phys.* **2013**, *138*, 024701.

(14) Ni, J.; Zhao, Y.; Li, L.; Mai, L. Ultrathin MoO2 Nanosheets for Superior Lithium Storage. *Nano Energy* **2015**, *11*, 129−135.

(15) Eivari, H. A.; Ghasemi, S. A.; Tahmasbi, H.; Rostami, S.; Faraji, S.; Rasoulkhani, R.; Goedecker, S.; Amsler, M. Two-Dimensional Hexagonal Sheet of TiO2. *Chem. Mater.* **2017**, *29*, 8594−8603.

(16) Xiao, J.; Choi, D.; Cosimbescu, L.; Koech, P.; Liu, J.; Lemmon, J. P. Exfoliated MoS2 Nanocomposite as an Anode Material for Lithium Ion Batteries. *Chem. Mater.* **2010**, *22*, 4522−4524.

(17) Bhandavat, R.; David, L.; Singh, G. Synthesis of Surface-Functionalized WS2 Nanosheets and Performance as Li-Ion Battery Anodes. *J. Phys. Chem. Lett.* **2012**, *3*, 1523−1530.

(18) Naguib, M.; Come, J.; Dyatkin, B.; Presser, V.; Taberna, P.-L.; Simon, P.; Barsoum, M. W.; Gogotsi, Y. MXene: A Promising Transition Metal Carbide Anode for Lithium-ion Batteries. *Electrochem. Commun.* **2012**, *16*, 61−64.

(19) Er, D.; Li, J.; Naguib, M.; Gogotsi, Y.; Shenoy, V. B. Ti3C2MXene as a High Capacity Electrode Material for Metal (Li, Na, K, Ca) Ion Batteries. *ACS Appl. Mater. Interfaces* **2014**, *6*, 11173−11179.

(20) Ugeda, M. M.; Bradley, A. J.; Shi, S.-F.; da Jornada, F. H.; Zhang, Y.; Qiu, D. Y.; Ruan, W.; Mo, S.-K.; Hussain, Z.; Shen, Z.-X.; Wang, F.; Louie, S. G.; Crommie, M. F. Giant Bandgap Renormalization and Excitonic Effects in a Monolayer Transition Metal Dichalcogenide Semiconductor. *Nat. Mater.* **2014**, *13*, 1091−1095.

(21) Qian, X.; Liu, J.; Fu, L.; Li, J. Quantum Spin Hall Effect in Two-Dimensional Transition Metal Dichalcogenides. *Science* **2014**, *346*, 1344−1347.

(22) Wang, Q. H.; Kalantar-Zadeh, K.; Kis, A.; Coleman, J. N.; Strano, M. S. Electronics and Optoelectronics of Two-Dimensional Transition Metal Dichalcogenides. *Nat. Nanotechnol.* **2012**, *7*, 699−712.

(23) Radisavljevic, B.; Kis, A. Mobility Engineering and a Metal−Insulator Transition in Monolayer MoS_2. *Nat. Mater.* **2013**, *12*, 815−820.

(24) Mak, K. F.; He, K.; Lee, C.; Lee, G. H.; Hone, J.; Heinz, T. F.; Shan, J. Tightly Bound Trions in Monolayer MoS_2. *Nat. Mater.* **2013**, *12*, 207−211.

(25) Peng, L.; Zhu, Y.; Chen, D.; Ruoff, R. S.; Yu, G. Two-Dimensional Materials for Beyond-Lithium-Ion Batteries. *Adv. Energy Mater.* **2016**, *6*, 1600025−1600045.

DOI: 10.1021/acs.chemmater.7b03997
Chem. Mater. 2017, 29, 9819−9828

(26) Yang, S.; Feng, X.; Ivanovici, S.; Müllen, K. Fabrication of Graphene-Encapsulated Oxide Nanoparticles: Towards High-Performance Anode Materials for Lithium Storage. *Angew. Chem., Int. Ed.* **2010**, *49*, 8408−8411.
(27) Yu, Z.; Tetard, L.; Zhai, L.; Thomas, J. Supercapacitor Electrode Materials: Nanostructures from 0 to 3 Dimensions. *Energy Environ. Sci.* **2015**, *8*, 702−730.
(28) Lebègue, S.; Björkman, T.; Klintenberg, M.; Nieminen, R. M.; Eriksson, O. Two-Dimensional Materials from Data Filtering and Ab Initio Calculations. *Phys. Rev. X* **2013**, *3*, 031002.
(29) Ashton, M.; Paul, J.; Sinnott, S. B.; Hennig, R. G. Topology-Scaling Identification of Layered Solids and Stable Exfoliated 2D Materials. *Phys. Rev. Lett.* **2017**, *118*, 106101.
(30) Mounet, N.; Gibertini, M.; Schwaller, P.; Merkys, A.; Castelli, I. E.; Cepellotti, A.; Pizzi, G.; Marzari, N. Novel Two-Dimensional Materials from High-Throughput Computational Exfoliation of Experimentally Known Compounds. 2016, arXiv: 1611.05234. arXiv.org ePrint archive.
(31) Clarke, S. M.; Walsh, J. P. S.; Amsler, M.; Malliakas, C. D.; Yu, T.; Goedecker, S.; Wang, Y.; Wolverton, C.; Freedman, D. E. Discovery of a Superconducting CuBi Intermetallic Compound by High-Pressure Synthesis. *Angew. Chem., Int. Ed.* **2016**, *55*, 13446−13449.
(32) Guo, K.; Akselrud, L.; Bobnar, M.; Burkhardt, U.; Schmidt, M.; Zhao, J.-T.; Schwarz, U.; Grin, Y. Weak Interactions under Pressure: hp-CuBi and Its Analogues. *Angew. Chem., Int. Ed.* **2017**, *56*, 5620−5624.
(33) Clarke, S. M.; Amsler, M.; Walsh, J. P. S.; Yu, T.; Wang, Y.; Meng, Y.; Jacobsen, S. D.; Wolverton, C.; Freedman, D. E. Creating Binary Cu−Bi Compounds Via High-Pressure Synthesis: A Combined Experimental and Theoretical Study. *Chem. Mater.* **2017**, *29*, 5276−5285.
(34) Chang, L. S.; Straumal, B. B.; Rabkin, E.; Gust, W.; Sommer, F. The Solidus Line of the Cu−Bi Phase Diagram. *J. Phase Equilib.* **1997**, *18*, 128−135.
(35) Amsler, M.; Wolverton, C. Dense Superconducting Phases of Copper-Bismuth at High Pressure. *Phys. Rev. Mater.* **2017**, *1*, 031801.
(36) Matthias, B. T.; Jayaraman, A.; Geballe, T. H.; Andres, K.; Corenzwit, E. Many More Superconducting Bismuth Phases. *Phys. Rev. Lett.* **1966**, *17*, 640−643.
(37) Naka, S.; Horii, K.; Takeda, Y.; Hanawa, T. Direct Conversion of Graphite to Diamond Under Static Pressure. *Nature* **1976**, *259*, 38−39.
(38) Eremets, M. I.; Gavriliuk, A. G.; Trojan, I. A.; Dzivenko, D. A.; Boehler, R. Single-Bonded Cubic Form of Nitrogen. *Nat. Mater.* **2004**, *3*, 558−563.
(39) Rêgo, C. R. C.; Oliveira, L. N.; Tereshchuk, P.; Da Silva, J. L. F. Comparative Study of van der Waals Corrections to the Bulk Properties of Graphite. *J. Phys.: Condens. Matter* **2015**, *27*, 415502.
(40) Carrete, J.; Li, W.; Lindsay, L.; Broido, D. A.; Gallego, L. J.; Mingo, N. Physically Founded Phonon Dispersions of Few-Layer Materials and the Case of Borophene. *Mater. Res. Lett.* **2016**, *4*, 204−211.
(41) Bahmann, S.; Weißbach, T.; Kortus, J. Crossed Graphene: Stability and Electronic Structure. *Phys. Status Solidi RRL* **2013**, *7*, 639−642.
(42) Björkman, T.; Gulans, A.; Krasheninnikov, A. V.; Nieminen, R. M. van der Waals Bonding in Layered Compounds from Advanced Density-Functional First-Principles Calculations. *Phys. Rev. Lett.* **2012**, *108*, 235502.
(43) Grimme, S. Semiempirical GGA-Type Density Functional Constructed with a Long-Range Dispersion Correction. *J. Comput. Chem.* **2006**, *27*, 1787−1799.
(44) Grimme, S.; Antony, J.; Ehrlich, S.; Krieg, S. A Consistent and Accurate Ab Initio Parametrization of Density Functional Dispersion Correction (DFT-D) for the 94 Elements H-Pu. *J. Chem. Phys.* **2010**, *132*, 154104.
(45) Grimme, S.; Ehrlich, S.; Goerigk, L. Effect of the Damping Function in Dispersion Corrected Density Functional Theory. *J. Comput. Chem.* **2011**, *32*, 1456−1465.
(46) Bučko, T.; Lebègue, S.; Ángyán, J. G.; Hafner, J. Extending the Applicability of the Tkatchenko-Scheffler Dispersion Correction via Iterative Hirshfeld Partitioning. *J. Chem. Phys.* **2014**, *141*, 034114.
(47) Steinmann, S. N.; Corminboeuf, C. Comprehensive Benchmarking of a Density-Dependent Dispersion Correction. *J. Chem. Theory Comput.* **2011**, *7*, 3567−3577.
(48) Jiang, D.; Du, M.-H.; Dai, S. First Principles Study of the Graphene/Ru(0001) Interface. *J. Chem. Phys.* **2009**, *130*, 074705.
(49) Lebègue, S.; Harl, J.; Gould, T.; Ángyán, J. G.; Kresse, G.; Dobson, J. F. Cohesive Properties and Asymptotics of the Dispersion Interaction in Graphite by the Random Phase Approximation. *Phys. Rev. Lett.* **2010**, *105*, 196401.
(50) Şahin, H.; Cahangirov, S.; Topsakal, M.; Bekaroglu, E.; Akturk, E.; Senger, R. T.; Ciraci, S. Monolayer Honeycomb Structures of Group-IV Elements and III-V Binary Compounds: First-principles Calculations. *Phys. Rev. B: Condens. Matter Mater. Phys.* **2009**, *80*, 155453.
(51) Zacharia, R.; Ulbricht, H.; Hertel, T. Interlayer Cohesive Energy of Graphite from Thermal Desorption of Polyaromatic Hydrocarbons. *Phys. Rev. B: Condens. Matter Mater. Phys.* **2004**, *69*, 155406.
(52) Benedict, L. X.; Chopra, N. G.; Cohen, M. L.; Zettl, A.; Louie, S. G.; Crespi, V. H. Microscopic Determination of the Interlayer Binding Energy in Graphite. *Chem. Phys. Lett.* **1998**, *286*, 490−496.
(53) Bonaccorso, F.; Colombo, L.; Yu, G.; Stoller, M.; Tozzini, V.; Ferrari, A. C.; Ruoff, R. S.; Pellegrini, V. Graphene, Related Two-Dimensional Crystals, and Hybrid Systems for Energy Conversion and Storage. *Science* **2015**, *347*, 1246501.
(54) Kim, H.; Park, K.-Y.; Hong, J.; Kang, K. All-Graphene-Battery: Bridging the Gap Between Supercapacitors and Lithium Ion Batteries. *Sci. Rep.* **2015**, *4*, 0278.
(55) Zhou, J.; Sun, Q.; Wang, Q.; Jena, P. Tailoring Li Adsorption on Graphene. *Phys. Rev. B: Condens. Matter Mater. Phys.* **2014**, *90*, 205427.
(56) Leggesse, E. G.; Chen, C.-L.; Jiang, J.-C. Lithium Diffusion in Graphene and Graphite: Effect of Edge Morphology. *Carbon* **2016**, *103*, 209−216.
(57) Park, M.; Zhang, X.; Chung, M.; Less, G. B.; Sastry, A. M. A Review of Conduction Phenomena in Li-ion Batteries. *J. Power Sources* **2010**, *195*, 7904−7929.
(58) Nitta, N.; Wu, F.; Lee, J. T.; Yushin, G. Li-ion Battery Materials: Present and Future. *Mater. Today* **2015**, *18*, 252−264.
(59) Zhou, X.; Wang, F.; Zhu, Y.; Liu, Z. Graphene Modified LiFePO4 Cathode Materials for High Power Lithium Ion Batteries. *J. Mater. Chem.* **2011**, *21*, 3353−3358.
(60) Jaber-Ansari, L.; Puntambekar, K. P.; Kim, S.; Aykol, M.; Luo, L.; Wu, J.; Myers, B. D.; Iddir, H.; Russell, J. T.; Saldaña, S. J.; Kumar, R.; Thackeray, M. M.; Curtiss, L. A.; Dravid, V. P.; Wolverton, C.; Hersam, M. C. Suppressing Manganese Dissolution from Lithium Manganese Oxide Spinel Cathodes with Single-Layer Graphene. *Adv. Energy Mater.* **2015**, *5*, 1500646−1500655.
(61) Blöchl, P. E. Projector Augmented-Wave Method. *Phys. Rev. B: Condens. Matter Mater. Phys.* **1994**, *50*, 17953−17979.
(62) Kresse, G. Ab-Initio Molecular-Dynamics for Liquid-Metals. *J. Non-Cryst. Solids* **1995**, *192-193*, 222−229.
(63) Kresse, G.; Furthmüller, J. Efficiency of Ab-Initio Total Energy Calculations for Metals and Semiconductors Using a Plane-Wave Basis Set. *Comput. Mater. Sci.* **1996**, *6*, 15−50.
(64) Kresse, G.; Joubert, D. From Ultrasoft Pseudopotentials to the Projector Augmented-Wave Method. *Phys. Rev. B: Condens. Matter Mater. Phys.* **1999**, *59*, 1758−1775.
(65) Perdew, J. P.; Burke, K.; Ernzerhof, M. Generalized Gradient Approximation Made Simple. *Phys. Rev. Lett.* **1996**, *77*, 3865−3868.
(66) Becke, A. D.; Edgecombe, K. E. A Simple Measure of Electron Localization in Atomic and Molecular Systems. *J. Chem. Phys.* **1990**, *92*, 5397−5403.
(67) Togo, A.; Oba, F.; Tanaka, I. First-Principles Calculations of the Ferroelastic Transition Between Rutile-Type and $CaCl_2$-Type SiO_2 at

DOI: 10.1021/acs.chemmater.7b03997
Chem. Mater. 2017, 29, 9819−9828

High Pressures. *Phys. Rev. B: Condens. Matter Mater. Phys.* **2008**, *78*, 134106.
(68) Giannozzi, P.; Baroni, S.; Bonini, N.; Calandra, M.; Car, R.; Cavazzoni, C.; Ceresoli, D.; Chiarotti, G. L.; Cococcioni, M.; Dabo, I.; Dal Corso, A.; de Gironcoli, S.; Fabris, S.; Fratesi, G.; Gebauer, R.; Gerstmann, U.; Gougoussis, C.; Kokalj, A.; Lazzeri, M.; Martin-Samos, L.; Marzari, N.; Mauri, F.; Mazzarello, R.; Paolini, S.; Pasquarello, A.; Paulatto, L.; Sbraccia, C.; Scandolo, S.; Sclauzero, G.; Seitsonen, A. P.; Smogunov, A.; Umari, P.; Wentzcovitch, R. M. QUANTUM ESPRESSO: a Modular and Open-Source Software Project for Quantum Simulations of Materials. *J. Phys.: Condens. Matter* **2009**, *21*, 395502.
(69) Allen, P. B.; Dynes, R. C. Transition Temperature of Strong-Coupled Superconductors Reanalyzed. *Phys. Rev. B* **1975**, *12*, 905–922.
(70) Yao, Z.; Kim, S.; Aykol, M.; Li, Q.; Wu, J.; He, J.; Wolverton, C. Revealing the Conversion Mechanism of Transition Metal Oxide Electrodes during Lithiation from First-Principles.*Chem. Mater.*,**2017**.10.1021/acs.chemmater.7b02058
(71) Li, Q.; Yao, Z.; Wu, J.; Mitra, S.; Hao, S.; Sahu, T. S.; Li, Y.; Wolverton, C.; Dravid, V. P. Intermediate Phases in Sodium Intercalation into MoS2 Nanosheets and their Implications for Sodium-Ion Batteries. *Nano Energy* **2017**, *38*, 342–349.
(72) He, K.; Yao, Z.; Hwang, S.; Li, N.; Sun, K.; Gan, H.; Du, Y.; Zhang, H.; Wolverton, C.; Su, D. Kinetically-Driven Phase Transformation during Lithiation in Copper Sulfide Nanoflakes. *Nano Lett.* **2017**, *17*, 5726–5733.
(73) Hart, G.; Forcade, R. Algorithm for Generating Derivative Structures. *Phys. Rev. B: Condens. Matter Mater. Phys.* **2008**, *77*, 224115–224126.
(74) Hart, G. L.; Nelson, L. J.; Forcade, R. W. Generating Derivative Structures at A Fixed Concentration. *Comput. Mater. Sci.* **2012**, *59*, 101–107.
(75) Thonhauser, T.; Cooper, V. R.; Li, S.; Puzder, A.; Hyldgaard, P.; Langreth, D. C. Van der Waals Density Functional: Self-Consistent Potential and the Nature of the van der Waals Bond. *Phys. Rev. B: Condens. Matter Mater. Phys.* **2007**, *76*, 125112–125122.
(76) Aydinol, M. K.; Kohan, A. F.; Ceder, G.; Cho, K.; Joannopoulos, J. Ab Initio Study of Lithium Intercalation in Metal Oxides and Metal Dichalcogenides. *Phys. Rev. B: Condens. Matter Mater. Phys.* **1997**, *56*, 1354–1365.
(77) Chan, M. K. Y.; Wolverton, C.; Greeley, J. P. First Principles Simulations of the Electrochemical Lithiation and Delithiation of Faceted Crystalline Silicon. *J. Am. Chem. Soc.* **2012**, *134*, 14362–14374.
(78) Kyle Michel, C. W., Logan Ward Materials Interface. https://github.com/materials/mint, 2015.
(79) Michel, K. J.; Zhang, Y.; Wolverton, C. Fast Mass Transport Kinetics in B20H16: A High-Capacity Hydrogen Storage Material. *J. Phys. Chem. C* **2013**, *117*, 19295–19301.
(80) Henkelman, G.; Jónsson, H. Improved Tangent Estimate in the Nudged Elastic Band Method for Finding Minimum Energy Paths and Saddle Points. *J. Chem. Phys.* **2000**, *113*, 9978–9985.
(81) Michel, K. J.; Wolverton, C. Symmetry Building Monte Carlo-based Crystal Structure Prediction. *Comput. Phys. Commun.* **2014**, *185*, 1389–1393.
(82) Li, Q.; Liu, H.; Yao, Z.; Cheng, J.; Li, T.; Li, Y.; Wolverton, C.; Wu, J.; Dravid, V. P. Electrochemistry of Selenium with Sodium and Lithium: Kinetics and Reaction Mechanism. *ACS Nano* **2016**, *10*, 8788–8795.

DOI: 10.1021/acs.chemmater.7b03997
Chem. Mater. 2017, 29, 9819–9828